Advances in Materials Research, *Vol. 14, No. 2 (2025) 99-123*
https://doi.org/10.12989/amr.2025.14.2.099

Free vibration analysis of FG plates with volume fraction-dependent porosity

Ahmed Amine Daikh*[1,2], Amine Chergui[3], Abdessamed Amara[3], Azzedine Brik[3], Mohamed Ouejdi Belarbi[4], Mohamed Sid Ahmed Houari[2], Azza M. Abdraboh[5] and Mohamed A. Eltaher[6,7]

[1]*Artificial Intelligence Laboratory for Mechanical and Civil Structures, and Soil, University Centre of Naama, P.O. Box 66, Naama 45000, Algeria*
[2]*Laboratoire d'Etude des Structures et de Mécanique des Matériaux, Département de Génie Civil, Faculté des Sciences et de la Technologie, Université Mustapha Stambouli B.P. 305, R.P.29000 Mascara, Algérie*
[3]*Department of Mechanical Engineering, University Centre of Naama, 45000, Algeria*
[4]*Laboratoire de Recherche en Génie Civil, LRGC, Université de Biskra, B.P. 145, R.P. 07000, Biskra, Algeria*
[5]*Physics Department, Faculty of science, Benha university, Benha, Egypt*
[6]*Faculty of Engineering, Mechanical Engineering Department, King Abdulaziz University, P.O. Box 80204, Jeddah, Saudi Arabia*
[7]*Faculty of Engineering, Mechanical Design and Production Department, Zagazig University, P.O. Box 44519, Zagazig, Egypt*

(*Received January 13, 2024, Revised September 5, 2024, Accepted February 12, 2025*)

Abstract. This study presents a corrigendum regarding the inclusion of porosity in functionally graded structures. Typically, researchers incorporate the porosity function into the rule of mixture without accounting for specific fabrication steps, which relate to the proportions of the material constituents as represented by the volume fraction. This paper investigates the free vibration of functionally graded plates analytically and proposes a novel approach to porosity inclusion, where the porosity function is directly related to the volume fraction. Tow schemes of porosity are analysed, volume fraction porosity-dependent (VFD) and rule of mixture porosity dependent (RMD). Four types of porosity are proposed, Even, Uneven, linear (1) and linear (2). Based on the generalized field of displacement, a new higher-order shear deformation theory is proposed in this work. The equilibrium equations are performed on the basis of the virtual work principle, and solved by applying Galerkin method to cover various boundary conditions. The influence of the structure geometry, materials combination parameter, type of porosity, and different boundary conditions on the vibration frequency of the FG plate is investigated in detail.

Keywords: functionally graded plate; Galerkin method; higher-order shear deformation plate theory; rule of mixture porosity dependent (RMD); vibration behavior; volume fraction porosity-dependent (VFD)

1. Introduction

Functionally graded material (FGM) is a sophisticated material that exhibits a smooth and

*Corresponding author, Ph.D., Professor, E-mail: aadaikh@cuniv-naama.dz

http://www.techno-press.org/?journal=amr&subpage=5 ISSN: 2234-0912 (Print), 2234-179X (Online)

continuous variation in its properties across the thickness of structures (Garg *et al*. 2021, Daikh *et al*. 2023). FGM are particularly noteworthy for their ability to mitigate stress concentration and prevent delamination phenomena (Khechai *et al*. 2015, Hirane *et al*. 2021). Due to these remarkable attributes, FGMs have found extensive applications in diverse fields, including nuclear power, aerospace engineering, chemistry, construction, mechanical engineering and other fields. However, porosities might arise within FGMs during their fabrication, resulting from significant differences in solidification temperatures between the two monolithic materials (Saleh *et al*. 2020, Zhu *et al* 2001). These porosities have a detrimental impact on the stiffness and structural performance of FGM components. Therefore, it becomes imperative to account for the porosity effect on the mechanical behavior while designing FGM structures. For this type of FGM structure, several researches have been performed to analyse the mechanical and dynamic behavior of FGM structures with or without porosities (Vinh *et al*. 2023, Daikh *et al*. 2023, Belarbi *et al*. 2023, Hai *et al*. 2023 and Mohamed *et al*. 2023). For instance, thermal-based vibration analysis of porous FGM plates was conducted by Zhou *et al*. (2018) using the first-order shear deformation theory (FSDT). Li *et al*. (2019) provided semi-analytical solutions for vibration analysis of porous FG cylindrical shells. Zhang *et al*. (2020) employed the Fourier-Ritz method, coupled with FSDT, to investigate the free vibration and damping responses of porous sandwich FGM plates with a viscoelastic core.

Yahia and his colleagues (2015) conducted a wave propagation analysis on porous functionally graded plates, employing various higher-order shear deformation theories (HSDT). In a similar vein, Barati and Shahverdi (2017) introduced a refined HSDT within the framework of the Galerkin method to investigate the stability of porous FG plates under aero-hygro-thermo-mechanical conditions. Another approach based on the sinusoidal shear deformation theory (SSDT) was presented by Demirhan and Taskin (2019), focusing on the free vibration and bending analysis of porous FG Levy's type plates. Based on high-order gradient continuity and higher-order Cauchy–Born rule, the mechanical response of microtubules are illustrated by Xiang *et al*. (2016) using developed meshfree computational framework.Daikh and Zenkour (2019) proposed a novel HSDT to explore the free vibration and buckling behaviors of power-law and sigmoidal simply supported porous FG sandwich plates. Based on the symplectic superposition method (SSM), Hu *et al*. (2023) developed a novel analytic solutions for free vibrationof non-Lévy-type porous FG plates. In another study by Zenkour and Aljadani (2019), they conducted a thermal buckling analysis of porous piezoelectric functionally graded nanoplates using HSDT. The porosity effect on the bending and free vibration response of FG plates in a thermal environment was analyzed by Gupta and Talha (2018). Shahsavari and his colleagues (2018) proposed a new quasi-3D hyperbolic shear deformation theory for analyzing the free vibration of FG porous plates resting on elastic foundations. According to a seventh-order shear deformation plate theory associated with the modified couple stress theory, Thanh *et al*. (2019) investigated the size-dependent effects on thermal buckling and post-buckling behaviors of porous FG microplates using the IGA. On the basis on HSDT, Merdaci and Belghoul (2019) explored the static behavior of porous functionally graded thick rectangular plates. Buckling of bi-coated FG porous nanoplates was studied by Daikh *et al*. (2023) and his collaborators using nonlocal strain gradient quasi-3D higher-order shear deformation plate theory. Based on classical beam theory (CBT) and FSDT, Avcar (2019) carried out a free vibration analysis of imperfect FGM beam including porosities. A three-dimensional Isogeometric analysis (IGA) numerical solution proposed by Thanh *et al*. (2021) for free vibration and buckling of FG porous annular plates, conical and cylindrical shells.

The free vibration analysis of FG carbon nanotube reinforced composite conical shell is examined by Xiang *et al*. (2021) using the element-free kp-Ritz method the first-order shear

deformation shell theory. Van Vinh *et al*. (2022) analyzed the bending and buckling response of 2D-FG porous plates using an improved first-order shear deformation theory and finite element method. Based on the Reissner-Mindlin plate theory and the Von-Kármán strain assumption, Cuong-Le *et al*. (2022) examined the linear/nonlinear bending of porous sigmoid FG nanoplates using the strain gradient theory and isogeometric finite element formulation. Based on Reddy higher-order plate theory coupled and isogeometric analysis, the nonlinear static bending response of porous FG micro-plate is studied by Thranh *et al*. (2022) using the Von-Kármán hypothesis and the modified couple stress theory. Based on FSDT and modified nonlocal elasticity theory, Van Vinh *et al*. (2023) examined the free vibration behavior of FG porous doubly curved shallow nanoshells with variable nonlocal parameters using FSDT. Based on a combination of generalized layerwise theory for higher-order shear deformation theory and the meshless radial point interpolation method, the free vibration and bending of laminated plates on Winkler foundations are investigated by Xia *et al*. (2022). The governing equations of motion are solved analytically using the Navier's solution. Belarbi *et al*. (2022) developed an efficient eight-node isoparametric element, based on layerwise approach, for the bending and free vibration analysis of porous FG sandwich plates with various porosity distributions. Xue *et al*. (2019) studied the free vibration response of porous FGM plates by employing an isogeometric analysis (IGA) method. Rezaei *et al*. (2017) used Levy's method based on FSDT to determine the natural frequencies of FG porous plates. Tran *et al*. (2021) studied the bending and free vibration responses of FGM porous variable-thickness plates using an edge-based smoothed finite element method. Using the HSDT, the bending of China Railway Track System type II track laminated plates on elastic foundations and interlayer shearing performances are analyzed by Xia *et al*. (2024) utilizing meshfree radial point interpolation method (RPIM), which has the properties of the Kronecker function and discretizes the governing equations derived from HSDT. On the basis of IGA and Quasi-3D trigonometric shear deformable shell theory with five unknowns, Van Do and Lee (2023) examined the bending and instability response of porous FG cylindrical shells. Shahverdi and Barati (2017) presented a general nonlocal strain-gradient elasticity model, based on Galerkin's method, for vibration analysis of porous nano-scale plates on an elastic substrate.

According to the review mentioned earlier, it seems that there is an abundance of literature on FGM porous structures. However, the examination of FGM plates with porosity-dependent properties is not widely accessible in the literature, with only a few recent papers addressing this topic. Wang and Zu (2017) performed a study on the porosity-dependent nonlinear forced vibrations of FGM piezoelectric plates by employing both analytical and numerical methods. Li *et al*. (2020) investigated the static bending, free vibration and buckling behaviors of bi-directional functionally graded (2D-FG) plates with Porosity-dependent using first-order shear deformation theory (FSDT) as well as isogeometric analysis (IGA). Based on quasi-3D five unknowns shear deformation theory, Arshid *et al*. (2022) carried out porosity-dependent vibration analysis of FG sandwich microplates considering hygrothermal effect. Later, porosity-dependent free vibration and dynamic stability of FG nanofilms was analyzed by Barati (2018) using nonlocal strain gradient theory based on Galerkin's approach. Porosity-dependent mechanical behaviors of FGM plate was investigated by Bekkaye *et al*. (2020) using refined trigonometric shear deformation theory. Similarly, Gafour *et al*. (2020) proposed a new HSDT to study the porosity-dependent free vibration response of FG nanobeam using non-local shear deformation. By considering the geometrical nonlinearity with von Kármán strains and FSDT, Kumar and Harsha (2022) examined the vibrational characteristics of a FG sigmoid piezoelectric plate under both electrical and mechanical loading conditions, considering porous and non-porous plate configurations. More recently, Based on FSDT, Saffari *et al*. (2023)

studied a porosity-dependent wave propagation behavior of multi-directional FG nanoplate with nonlinear temperature-dependent characteristics on Kerr-type substrate.

In this paper, an attempt has been carried out to study the free vibration of FG plates by considering the porosity which is related to the volume fraction, in contrast to the performed researches in which the porosity is related to the rule of mixture. The formulations are performed based on the higher-order shear deformation theory, and Galerkin's procedure is employed to solve the equilibrium equations.

2. Material properties

A rectangular plate in the Cartesian coordinate system (x, y, z) with width $a \times b$ and thickness h is shown in Fig. 1. The plate is composed of ceramic and metal. The material properties vary continuously from the bottom surface to the top surface. In this work, two cases of material constituent's dependent on porosity are considered: dependence on the volume fraction of porosity (VFD) and dependence on the porosity mixing rule (RMD). The effective mechanical properties and volume fraction of functionally graded plates (FGM) taking into account the effect of porosity can be defined as follows:

2.1 Volume Fraction Porosity Dependent (VFD)

The volume fraction of the ceramic phase, including the effect of porosity, can be expressed as follows:

$$V(z) = \left(\frac{1}{2} + \frac{z}{h}\right)^{p} - \Theta(z) \tag{1}$$

where p and $\Theta(z)$ represent the power law index and the porosity distribution function, respectively. The effective mechanical properties, such as Young's modulus (E), mass density (ρ), and Poisson's ratio (υ), can be described by the mixing rule as follows (Daikh *et al*. 2023):

$$P(x, z) = P_m + (P_c - P_m)V(x) \tag{2}$$

2.2 Rule Mixture Porosity Dependent (RMD)

In the case of porosity dependence according to the mixing rule, the volume fraction of the ceramic phase in the x direction can be calculated as follows (Wu *et al*. 2003):

$$V(z) = \left(\frac{1}{2} + \frac{z}{h}\right)^{p} \tag{3}$$

where the mixing rule is given by:

$$P(z) = P_m + (P_c - P_m)V(z) - \Theta(z) \tag{4}$$

In the given context, P_m and P_c represent the mechanical properties (such as Young's modulus, density, etc.) of the metal and ceramic constituents, respectively. $V(z)$ represents the volume fraction of the ceramic phase in the x and z directions.

Four types of porosity distributions have been examined: Even distribution, uneven distribution, linear (1) distribution, and linear (2) distribution. The function that defines the porosity can be

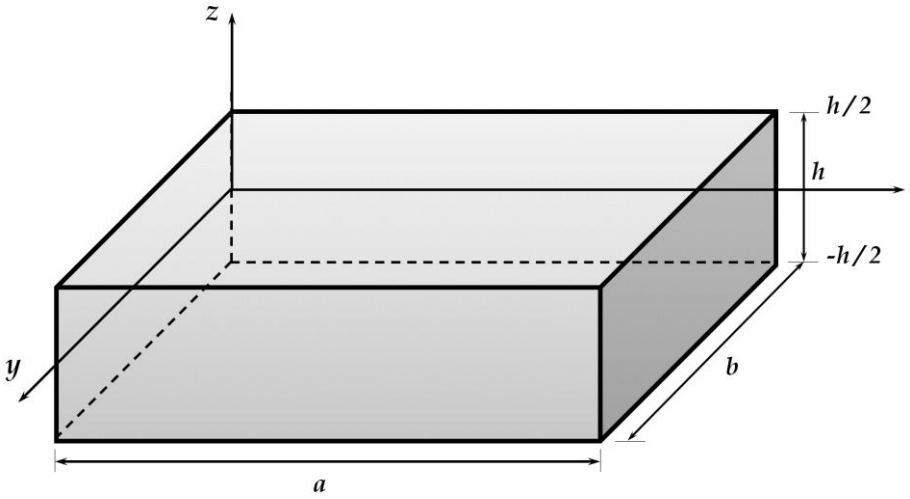

Fig. 1 Geometry of the FG plate

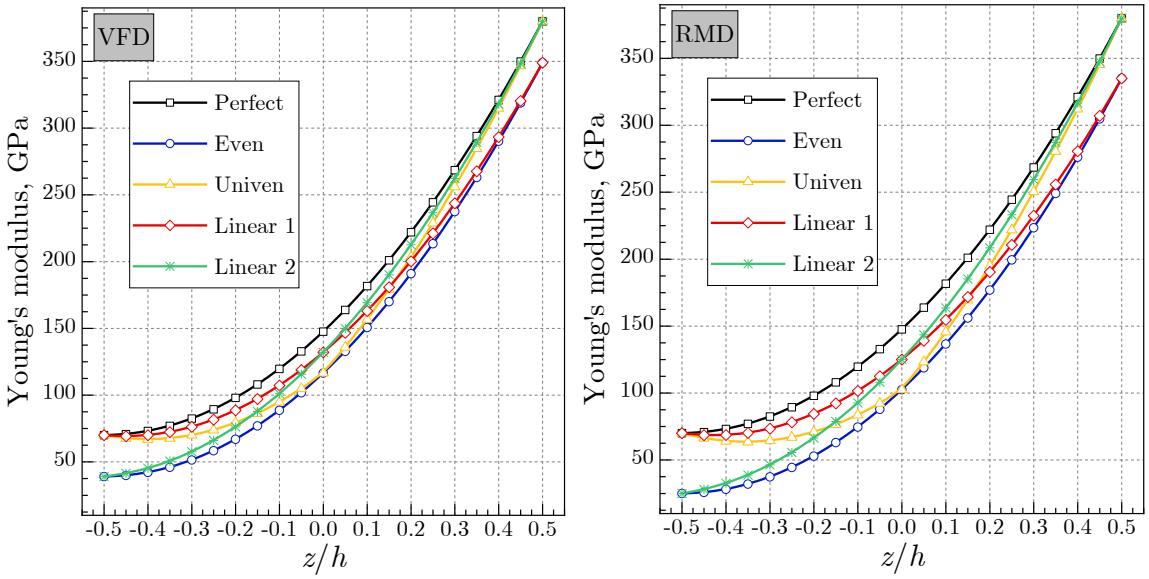

Fig. 2 The effect of the porosity scheme on Young's modulus ($p = 2, \xi = 0.2$)

expressed as follows (Barati 2018, Ghandourah *et al*. 2023):

• For Even porosity:

$$\Theta(z) = \frac{\xi}{2} \tag{5}$$

• For uneven porosity:

$$\Theta(z) = \frac{\xi}{2}\left(1 - \frac{2|z|}{h}\right) \tag{6}$$

• For linear (1) porosity:

$$\Theta(z) = \frac{\xi}{2}\left(\frac{1}{2} + \frac{z}{h}\right) \tag{7}$$

• For linear (2) porosity:

$$\Theta(z) = \frac{\xi}{2}\left(\frac{2z-1}{2h}\right) \tag{8}$$

The porosity coefficient is defined by the symbol ξ, where $0 \leq \xi \leq 0.2$. A comparison analysis between the effect of the first porosity scheme "VFD" and the other "RMD" on the Young's modulus of the FGM plate is plotted in Fig. 2, considering the different types of porosity. It is clear that "RMD" has a greater influence on the elastic modulus compared to "VFD".

3. Displacement field

The governing equations for the dynamic response of FGM plates are derived using a shear deformation theory based on an inverse trigonometric function. The displacement field is defined as follows:

$$\begin{aligned} u(x,y,z,t) &= u_0 - z\frac{\partial w_0}{\partial x} + f(z)\psi_x \\ v(x,y,z,t) &= v_0 - z\frac{\partial w_0}{\partial y} + f(z)\psi_y \\ w(x,y,z,t) &= w_0 \end{aligned} \tag{9}$$

The displacements of the mid-plane of the composite plate are denoted as u_0, v_0, and w_0, and the transverse normal rotations at $z = 0$ are noted as ψ_x and ψ_y. The shape function f(z) is given by (Ghandourah *et al*. 2023):

$$f(z) = 5h\,\mathrm{atan}\left(\frac{z}{h}\right) - 4z \tag{10}$$

The strains can be obtained by differentiating the displacement equation given above:

$$\begin{aligned} \begin{Bmatrix} \varepsilon_{xx} \\ \varepsilon_{yy} \\ \gamma_{xy} \end{Bmatrix} &= \begin{Bmatrix} \varepsilon_{xx}^0 \\ \varepsilon_{yy}^0 \\ \gamma_{xy}^0 \end{Bmatrix} + z\begin{Bmatrix} \varepsilon_{xx}^1 \\ \varepsilon_{yy}^1 \\ \gamma_{xy}^1 \end{Bmatrix} + f(z)\begin{Bmatrix} \varepsilon_{xx}^2 \\ \varepsilon_{yy}^2 \\ \gamma_{xy}^2 \end{Bmatrix} \\ \varepsilon_{zz} = 0, \quad \begin{Bmatrix} \gamma_{yz} \\ \gamma_{xz} \end{Bmatrix} &= \frac{\mathrm{d}f(z)}{\mathrm{d}z}\begin{Bmatrix} \gamma_{yz}^0 \\ \gamma_{xz}^0 \end{Bmatrix}, \end{aligned} \tag{11}$$

where

$$\begin{Bmatrix} \varepsilon_{xx}^0 \\ \varepsilon_{yy}^0 \\ \gamma_{xy}^0 \end{Bmatrix} = \begin{Bmatrix} \dfrac{\partial u_0}{\partial x} \\ \dfrac{\partial v_0}{\partial y} \\ \dfrac{\partial v_0}{\partial x} + \dfrac{\partial u_0}{\partial y} \end{Bmatrix}, \quad \begin{Bmatrix} \varepsilon_{xx}^1 \\ \varepsilon_{yy}^1 \\ \gamma_{xy}^1 \end{Bmatrix} = -\begin{Bmatrix} \dfrac{\partial^2 w_0}{\partial x^2} \\ \dfrac{\partial^2 w_0}{\partial y^2} \\ 2\dfrac{\partial^2 w_0}{\partial x \partial y} \end{Bmatrix} \tag{12}$$

$$\begin{Bmatrix} \varepsilon_{xx}^2 \\ \varepsilon_{yy}^2 \\ \gamma_{xy}^2 \end{Bmatrix} = \begin{Bmatrix} \dfrac{\partial \varphi_1}{\partial x} \\ \dfrac{\partial \varphi_2}{\partial y} \\ \dfrac{\partial \varphi_2}{\partial x} + \dfrac{\partial \varphi_1}{\partial y} \end{Bmatrix}, \quad \begin{Bmatrix} \gamma_{yz}^0 \\ \gamma_{xz}^0 \end{Bmatrix} = \begin{Bmatrix} \varphi_x \\ \varphi_y \end{Bmatrix}. \tag{12}$$

The stress-strain relationships are governed by:

$$\begin{Bmatrix} \sigma_{xx} \\ \sigma_{yy} \\ \tau_{yz} \\ \tau_{xz} \\ \tau_{xy} \end{Bmatrix} = \begin{bmatrix} Q_{11} & Q_{12} & 0 & 0 & 0 \\ Q_{12} & Q_{22} & 0 & 0 & 0 \\ 0 & 0 & Q_{44} & 0 & 0 \\ 0 & 0 & 0 & Q_{55} & 0 \\ 0 & 0 & 0 & 0 & Q_{66} \end{bmatrix} \begin{Bmatrix} \varepsilon_{xx} \\ \varepsilon_{yy} \\ \gamma_{yz} \\ \gamma_{xz} \\ \gamma_{xy} \end{Bmatrix} \tag{13}$$

where

$$Q_{11} = \frac{E}{1-\nu^2}\,, \qquad Q_{22} = Q_{11}\,, \qquad Q_{12} = \frac{\nu E}{1-\nu^2}, \qquad Q_{44} = Q_{55} = Q_{66} = \frac{E}{2(1+\nu)} \tag{14}$$

Here, ∇^2 denotes the Laplace operator $\left(\nabla^2 = \frac{\partial^2}{\partial x^2} + \frac{\partial^2}{\partial y^2}\right)$. Integrating Eq. (13**)** gives the stress relationships, moment, and additional moment resultants as follows:

$$\begin{Bmatrix} \{N\} \\ \{M\} \\ \{P\} \end{Bmatrix} = \begin{bmatrix} [A] & [B] & [C] \\ [B] & [D] & [F] \\ [C] & [F] & [H] \end{bmatrix} \begin{Bmatrix} \{\varepsilon^0\} \\ \{\varepsilon^1\} \\ \{\varepsilon^2\} \end{Bmatrix} \tag{15}$$

$$\begin{Bmatrix} R_{yz} \\ R_{xz} \end{Bmatrix} = \begin{bmatrix} J_{44} & J_{45} \\ J_{45} & J_{55} \end{bmatrix} \begin{Bmatrix} \gamma_{yz}^0 \\ \gamma_{xz}^0 \end{Bmatrix} \tag{16}$$

where

$$\begin{matrix} , & , \\ , & , \end{matrix} \tag{17}$$

$$\begin{matrix} \{N\} = \{N_{xx} & N_{yy} & N_{xy}\}^T \\ \{M\} = \{M_{xx} & M_{yy} & M_{xy}\}^T \\ \{P\} = \{P_{xx} & P_{yy} & P_{xy}\}^T \end{matrix} \tag{18a}$$

$$\begin{matrix} \{\varepsilon^0\} = \{\varepsilon_{xx}^0 & \varepsilon_{yy}^0 & \gamma_{xy}^0\}^T \\ \{\varepsilon^1\} = \{\varepsilon_{xx}^1 & \varepsilon_{yy}^1 & \gamma_{xy}^1\}^T \\ \{\varepsilon^2\} = \{\varepsilon_{xx}^2 & \varepsilon_{yy}^2 & \gamma_{xy}^2\}^T \end{matrix} \tag{18b}$$

$$\begin{aligned} &\{A_{ij}, B_{ij}, D_{ij}, C_{ij}, F_{ij}, H_{ij}\} \\ &= \int_{h_{n-1}}^{h_n} Q_{ij}\{1, z, z^2, f(z), zf(z), f(z)^2\}\mathrm{d}z\,, (i,j = 1,2,6) \\ &J_{ii} = \int_{h_{n-1}}^{h_n} Q_{ii}\left[\frac{\mathrm{d}f(z)}{\mathrm{d}z}\right]^2 \mathrm{d}z\,, (i = 4,5) \end{aligned} \tag{18c}$$

4. Governing equations

The equations of motion for the FGM plate are derived using the Hamilton's principle:

$$\delta \int_{t_2}^{t_1} \delta(U - T + V)dt \; = \; 0 \tag{19}$$

The strain energy of the FGM plate can be calculated as follows:

$$\delta U_p = \frac{1}{2}\int_V \left[\sigma_{xx}^{(k)}\delta\varepsilon_{xx} + \sigma_{yy}^{(k)}\delta\varepsilon_{xx} + \sigma_{xy}^{(k)}\delta\gamma_{xy} + \sigma_{xz}^{(k)}\delta\gamma_{xz} + \sigma_{yz}^{(k)}\delta\gamma_{yz}\right]\mathrm{d}V \tag{20}$$

The kinetic energy of the FGM plate at a given instant can be formulated as follows:

$$\delta T = \frac{1}{2}\int_0^L \int_A \rho(\dot{u}\delta\dot{u} + \dot{v}\delta\dot{v} + \dot{w}\delta\dot{w})\, dAdx \tag{21}$$

$$\begin{aligned}\delta T = \int_V \Big\{ & I_0(\dot{u}_0\delta\dot{u}_0 + \dot{v}_0\delta\dot{v}_0 + \dot{w}_0\delta\dot{w}_0) + I_1\left(\frac{\partial\dot{w}_0}{\partial x}\delta\dot{u}_0 + \frac{\partial\dot{w}_0}{\partial y}\delta\dot{v}_0 + \dot{u}_0\frac{\partial\delta\dot{w}_0}{\partial x} + \dot{v}_0\frac{\partial\delta\dot{w}_0}{\partial y}\right) \\ & + I_2\left(\frac{\partial\dot{w}_0}{\partial x}\frac{\partial\delta\dot{w}_0}{\partial x} + \frac{\partial\dot{w}_0}{\partial y}\frac{\partial\delta\dot{w}_0}{\partial y}\right) + I_3\left(\dot{\varphi}_x\delta\dot{u}_0 + \dot{u}_0\delta\dot{\varphi}_x + \dot{\varphi}_y\delta\dot{v}_0 + \dot{v}_0\delta\dot{\varphi}_y\right) \\ & + I_4\left(\dot{\varphi}_x\frac{\partial\delta\dot{w}_0}{\partial x} + \frac{\partial\dot{w}_0}{\partial x}\delta\dot{\varphi}_x + \dot{\varphi}_y\frac{\partial\delta\dot{w}_0}{\partial y} + \frac{\partial\dot{w}_0}{\partial y}\delta\dot{\varphi}_y\right) + I_5\left(\dot{\varphi}_x\delta\dot{\varphi}_x + \dot{\varphi}_y\delta\dot{\varphi}_y\right)\Big\}\mathrm{d}x\mathrm{d}y\mathrm{d}z\end{aligned} \tag{22}$$

where

$$\{I_0, I_1, I_2, I_3, I_4, I_5\} = \rho(z)\left\{1, z, z^2, \Phi(z), z\Phi(z), \left(\Phi(z)\right)^2\right\} dz \tag{23}$$

By substituting Eqs. (20) and (22) into Eq. (19), we obtain the equilibrium equations for the FGM plate as follows:

$$\begin{aligned}& A_{11}\frac{\partial^2 u_0}{\partial x^2} + A_{66}\frac{\partial^2 u_0}{\partial y^2} + (A_{12} + A_{66})\frac{\partial^2 v_0}{\partial x\partial y} - B_{11}\frac{\partial^3 w_0}{\partial x^3} - (B_{12} + 2B_{66})\frac{\partial^3 w_0}{\partial x\partial y^2} \\ & + B_{11}^s\frac{\partial^2\psi_x}{\partial x^2} + B_{66}^s\frac{\partial^2\psi_x}{\partial y^2} + (B_{12}^s + B_{66}^s)\frac{\partial^2\psi_y}{\partial x\partial y} = I_0\frac{\partial^2 u_0}{\partial t^2} - I_1\frac{\partial^3 w_0}{\partial x\partial t^2} + I_3\frac{\partial^2\psi_x}{\partial t^2}\end{aligned} \tag{24}$$

$$\begin{aligned}& (A_{12} + A_{66})\frac{\partial^2 u_0}{\partial x\partial y} + A_{22}\frac{\partial^2 v_0}{\partial y^2} + A_{66}\frac{\partial^2 v_0}{\partial x^2} - (B_{12} + 2B_{66})\frac{\partial^3 w_0}{\partial x^2\partial y} - B_{22}\frac{\partial^3 w_0}{\partial y^3} \\ & + (B_{12}^s + B_{66}^s)\frac{\partial^2\psi_x}{\partial x\partial y} + B_{22}^s\frac{\partial^2\psi_y}{\partial y^2} + B_{66}^s\frac{\partial^2\psi_y}{\partial x^2} = I_0\frac{\partial^2 v_0}{\partial t^2} - I_1\frac{\partial^3 w_0}{\partial y\partial t^2} + I_3\frac{\partial^2\psi_y}{\partial t^2}\end{aligned} \tag{25}$$

$$\begin{aligned}& B_{11}\frac{\partial^3 u_0}{\partial x^3} + (B_{12} + 2B_{66})\frac{\partial^3 u_0}{\partial x\partial y^2} + (B_{12} + 2B_{66})\frac{\partial^3 v_0}{\partial x^2\partial y} + B_{22}\frac{\partial^3 v_0}{\partial y^3} - D_{11}\frac{\partial^4 w_0}{\partial x^4} \\ & - (2D_{12} + 4D_{66})\frac{\partial^4 w_0}{\partial x^2\partial y^2} - D_{22}\frac{\partial^4 w_0}{\partial y^4} + D_{11}^s\frac{\partial^3\psi_x}{\partial x^3} + (D_{12}^s + 2D_{66}^s)\frac{\partial^3\psi_x}{\partial x\partial y^2} \\ & + (D_{12}^s + 2D_{66}^s)\frac{\partial^3\psi_y}{\partial x^2\partial y} + D_{22}^s\frac{\partial^3\psi_y}{\partial y^3} = I_0\frac{\partial^2 w_0}{\partial t^2} + I_1\frac{\partial^3 u_0}{\partial x\partial t^2} + I_1\frac{\partial^3 v_0}{\partial y\partial t^2} \\ & - I_2\left(\frac{\partial^4 w_0}{\partial x^2\partial t^2} + \frac{\partial^4 w_0}{\partial y^2\partial t^2}\right) + I_4\left(\frac{\partial^3\psi_x}{\partial x\partial t^2} + \frac{\partial^3\psi_y}{\partial y\partial t^2}\right)\end{aligned} \tag{26}$$

$$B_{11}^s\frac{\partial^2 u_0}{\partial x^2}+B_{66}^s\frac{\partial^2 u_0}{\partial y^2}+(B_{12}^s+B_{66}^s)\frac{\partial^2 v_0}{\partial x\partial y}-D_{11}^s\frac{\partial^3 w_0}{\partial x^3}-(D_{12}^s+2D_{66}^s)\frac{\partial^3 w_0}{\partial x\partial y^2}+F_{11}^s\frac{\partial^2 \psi_x}{\partial x^2}$$
$$+F_{66}^s\frac{\partial^2 \psi_x}{\partial y^2}-A_{44}^s\psi_x+(F_{12}^s+F_{66}^s)\frac{\partial^2 \psi_y}{\partial x\partial y}=I_3\frac{\partial^2 u_0}{\partial t^2}-I_4\frac{\partial^3 w_0}{\partial x\partial t^2}+I_5\frac{\partial^2 \psi_x}{\partial t^2} \quad (27)$$

$$(B_{12}^s+B_{66}^s)\frac{\partial^2 u_0}{\partial x\partial y}+B_{11}^s\frac{\partial^2 v_0}{\partial y^2}+B_{66}^s\frac{\partial^2 v_0}{\partial x^2}-(D_{12}^s+2D_{66}^s)\frac{\partial^3 w_0}{\partial x^2\partial y}-D_{22}^s\frac{\partial^3 w_0}{\partial y^3}$$
$$+(F_{12}^s+F_{66}^s)\frac{\partial^2 \psi_x}{\partial x\partial y}+F_{11}^s\frac{\partial^2 \psi_y}{\partial y^2}+F_{66}^s\frac{\partial^2 \psi_y}{\partial x^2}-A_{44}^s\psi_y=I_3\frac{\partial^2 v_0}{\partial t^2}-I_4\frac{\partial^3 w_0}{\partial y\partial t^2}+I_5\frac{\partial^2 \psi_y}{\partial t^2} \quad (28)$$

5. Analytical solution

This research aims to extend the application of analytical solutions to analyze the response of various structures, including plates, under different boundary conditions. To achieve this goal, the Galerkin approach is used to obtain accurate solutions. The generalized displacements can be represented as follows (Daikh *et al*. 2020, 2022):

$$\{u_0,\psi_x\}=\sum_{m=1}^{\infty}\sum_{n=1}^{\infty}\{U_{mn},X_{mn}\}\frac{\partial X_m(x)}{\partial x}Y_n(y)e^{i\omega t}$$
$$\{v_0,\psi_y\}=\sum_{m=1}^{\infty}\sum_{n=1}^{\infty}\{V_{mn},Z_{mn}\}X_m(x)\frac{\partial Y_n(y)}{\partial y}e^{i\omega t} \quad (29)$$
$$w_0=\sum_{m=1}^{\infty}\sum_{n=1}^{\infty}W_{mn}X_m(x)Y_n(y)\,e^{i\omega t}$$

U_{mn}, V_{mn}, W_{mn}, X_{mn} and Z_{mn} are arbitrary parameters. The functions $X_m(x)$ and $Y_n(y)$ that satisfy the simply supported and fixed boundary conditions (shown in Fig. 3) are expressed in Table 1.

Table 1 Admissible functions $X_m(x)$ and $Y_n(y)$

BCs.	Fonctions $X_m(x)$ and $Y_n(x)$	
	$X_m(x)$	$Y_n(y)$
SSSS	$\sin(\alpha x)$	$\sin(\beta y)$
CCCC	$\sin^2(\alpha x)$	$\sin^2(\beta y)$
CCSS	$\sin^2(\alpha x)$	$\sin(\beta y)$
SCSC	$\sin(\alpha x)[\cos(\alpha x)-1]$	$\sin(\beta y)[\cos(\beta y)-1]$

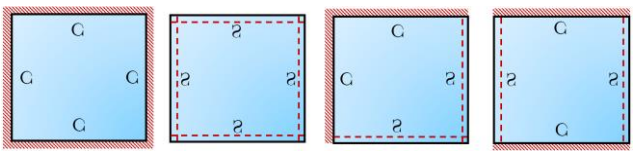

Fig. 3 Different boundary conditions

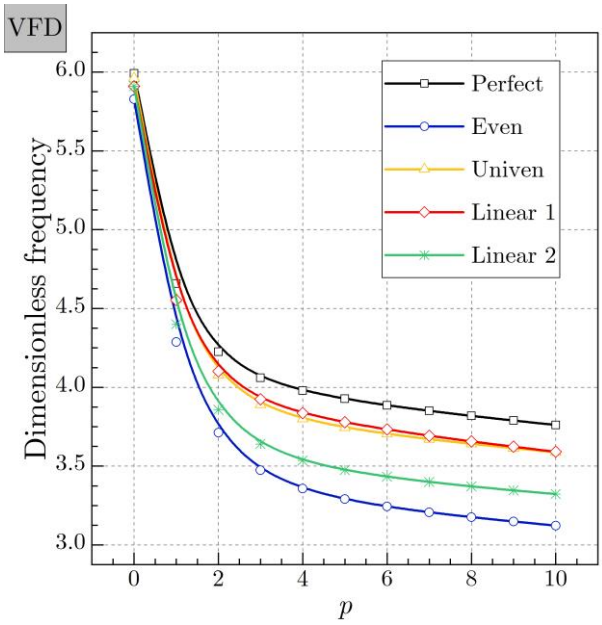

Fig. 4 The effect of the power index "p" and porosity type on the dimensionless frequency (VFD, $a = b = 10h,\ \xi = 0.2, SSSSn = m = 1$)

where $\lambda = m\pi/a$ and $\mu = n\pi/b$. Here, m and n represent the vibration modes.
By substituting Eq. (29) into Eqs. (44)-(48**)**, we obtain:

$$([K] - \omega_{mn}^2\,[M])\begin{Bmatrix} U_{mn} \\ V_{mn} \\ W_{mn} \\ X_{mn} \\ Z_{mn} \end{Bmatrix} = 0 \tag{30}$$

where $[K]$ and $[M]$ are the stiffness matrix and mass matrix, respectively.

The elements K_{ij} and M_{ij} of the matrices [K] and [M] are provided in Appendix A.

6. Results and discussions

Let's consider an FGM plate under different boundary conditions, composed of a mixture of metal and ceramic. The material combination consists of Aluminium alloy Al and Alumina Al_2O_3. Young's modulus and the density for the Aluminium are $E_m = 70\text{GPa}$ and $\rho_m = 2702\text{kg/cm}^3$, respectively, and for Alumina are $E_c = 380\text{GPa}$ and $\rho_c = 3800\text{kg/cm}^3$, respectively. The Poisson's ratio is constant ($\upsilon = 0.3$).

The normalized frequency results are calculated using the following expressions:

$$\bar{\omega} = \omega \frac{a^2}{h}\sqrt{\frac{\rho_c}{E_c}} \tag{31}$$

Table 2 Dimensionless natural frequencies of simply supported square porous RMD FG plates ($\bar{\omega} = \omega h\sqrt{\rho_m/E_m}$)

a/h	*p*	ξ	Even Porosity			Uneven Porosity		
			Belarbi *et al*. (2024)	Demirhan and Taskin (2019)	Present	Belarbi *et al*. (2024)	Demirhan and Taskin (2019)	Present
5	0	0.0	0.4153	0.4182	0.4150	0.4153	0.4182	0.4150
		0.2	0.4284	0.4313	0.4280	0.4257	0.4293	0.4253
		0.4	0.4475	0.4506	0.4471	0.4378	0.4423	0.4371
	0.1	0.0	0.4008	0.4032	0.4005	0.4008	0.4032	0.4005
		0.2	0.4115	0.4140	0.4112	0.4106	0.4137	0.4101
		0.4	0.4275	0.4299	0.4271	0.4219	0.4259	0.4213
	0.5	0.0	0.3554	0.3571	0.3551	0.3554	0.3571	0.3551
		0.2	0.3548	0.3563	0.3544	0.3618	0.3640	0.3613
		0.4	0.3519	0.3531	0.3514	0.3690	0.3722	0.3685
	1	0.0	0.3206	0.3225	0.3205	0.3206	0.3225	0.3205
		0.2	0.3052	0.3068	0.3051	0.3224	0.3250	0.3222
		0.4	0.2672	0.2683	0.2672	0.3235	0.3271	0.3233
10	0	0.0	0.1135	0.1137	0.1134	0.1135	0.1137	0.1134
		0.2	0.1170	0.1173	0.1169	0.1167	0.1170	0.1166
		0.4	0.1222	0.1225	0.1221	0.1205	0.1208	0.1203
	0.1	0.0	0.1092	0.1094	0.1092	0.1092	0.1094	0.1092
		0.2	0.1121	0.1123	0.1120	0.1123	0.1126	0.1122
		0.4	0.1164	0.1166	0.1163	0.1159	0.1162	0.1157
	0.5	0.0	0.0964	0.0965	0.0963	0.0964	0.0965	0.0963
		0.2	0.0960	0.0961	0.0959	0.0984	0.0986	0.0984
		0.4	0.0948	0.0949	0.0947	0.1009	0.1011	0.1008
	1	0.0	0.0869	0.0870	0.0868	0.0869	0.0870	0.0868
		0.2	0.0823	0.0824	0.0823	0.0877	0.0879	0.0876
		0.4	0.0713	0.0714	0.0713	0.0884	0.0887	0.0883
20	0	0.0	0.0291	0.0291	0.0291	0.0291	0.0291	0.0291
		0.2	0.0300	0.0300	0.0300	0.0300	0.0300	0.0299
		0.4	0.0314	0.0314	0.0313	0.0310	0.0310	0.0309
	0.1	0.0	0.0280	0.0280	0.0280	0.0280	0.0280	0.0280
		0.2	0.0287	0.0288	0.0287	0.0288	0.0288	0.0288
		0.4	0.0298	0.0298	0.0298	0.0298	0.0298	0.0298
	0.5	0.0	0.0247	0.0247	0.0246	0.0247	0.0247	0.0246
		0.2	0.0246	0.0246	0.0245	0.0252	0.0252	0.0252
		0.4	0.0242	0.0242	0.0242	0.0259	0.0259	0.0259
	1	0.0	0.0222	0.0222	0.0222	0.0222	0.0222	0.0222
		0.2	0.0210	0.0210	0.0210	0.0225	0.0225	0.0224
		0.4	0.0182	0.0182	0.0182	0.0227	0.0227	0.0227

Table 3 The effect of the power index "p" porosity coefficient, and porosity type on the dimensionless frequency ($a = b = 10h, SSSS, n = m = 1$)

ξ	p	VFD				RMD			
		Even	Uneven	Nlinear 1	Nlinear 2	Even	Uneven	Nlinear 1	Nlinear 2
0.00	0	5.7694	5.7694	5.7694	5.7694	5.7694	5.7694	5.7694	5.7694
	1	4.4193	4.4193	4.4193	4.4193	4.4193	4.4193	4.4193	4.4193
	2	4.0090	4.0090	4.0090	4.0090	4.0090	4.0090	4.0090	4.0090
	5	3.7683	3.7683	3.7683	3.7683	3.7683	3.7683	3.7683	3.7683
	10	3.6369	3.6369	3.6369	3.6369	3.6369	3.6369	3.6369	3.6369
0,05	0	5.7310	5.7638	5.7502	5.7502	5.8090	5.8082	5.7886	5.7886
	1	4.3321	4.3976	4.3966	4.3553	4.3759	4.4296	4.4282	4.3674
	2	3.8911	3.9758	3.9819	3.9192	3.9152	4.0006	4.0098	3.9167
	5	3.6307	3.7272	3.7356	3.6648	3.6438	3.7480	3.7608	3.6549
	10	3.5012	3.5973	3.5993	3.5399	3.5149	3.6186	3.6218	3.5326
0,10	0	5.6918	5.7581	5.7306	5.7306	5.8519	5.8485	5.8081	5.8081
	1	4.2405	4.3753	4.3735	4.2882	4.3244	4.4398	4.4374	4.3086
	2	3.7641	3.9413	3.9544	3.8232	3.8000	3.9901	4.0105	3.8096
	5	3.4796	3.6838	3.7022	3.5521	3.4848	3.7232	3.7525	3.5186
	10	3.3526	3.5554	3.5605	3.4336	3.3593	3.5954	3.6049	3.4055
0,15	0	5.6517	5.7524	5.7106	5.7106	5.8987	5.8902	5.8281	5.8281
	1	4.1439	4.3524	4.3500	4.2177	4.2626	4.4498	4.4470	4.2416
	2	3.6265	3.9054	3.9263	3.7203	3.6554	3.9772	4.0113	3.6842
	5	3.3116	3.6380	3.6681	3.4285	3.2738	3.6931	3.7435	3.3526
	10	3.1875	3.5108	3.5206	3.3163	3.1518	3.5660	3.5860	3.2478
0,20	0	5.6107	5.7466	5.6902	5.6902	5.9499	5.9334	5.8484	5.8484
	1	4.0416	4.3289	4.3262	4.1434	4.1875	4.4597	4.4569	4.1650
	2	3.4761	3.8680	3.8978	3.6096	3.4692	3.9615	4.0120	3.5360
	5	3.1218	3.5895	3.6332	3.2920	2.9780	3.6562	3.7335	3.1462
	10	3.0005	3.4630	3.4793	3.1858	2.8550	3.5282	3.5644	3.0477

Table 2 presents a comparative analysis of the dimensionless natural frequencies ($\bar{\omega} = \omega h\sqrt{\rho_m/E_m}$) of simply supported Al/Al_2O_3 FG square plate resting influenced by Even or Uneven porosity distribution. The power-law index values considered are p=0, 0.1, 0.5, 1, while the porosity coefficient while the porosity coefficient takes values of 0 (perfect), 0.2 and 0.4. The obtained results are compared with those obtained by Belarbi *et al*. (2024) using the FEM and an improved FSDT, and those obtained by Demirhan and Taskin using Lévy-type solution based on state-space approach and the sinusoidal shear deformation theory. The results show a strong agreement with those of Belarbi *et al*. (2024).

The following tables represent the numerical results of dimensionless frequencies influenced by the porosity coefficient "ξ" and power index "p" (Table 3), different boundary conditions, and geometric parameter "b/a" (Table 4), and the geometric parameter "a/h" (Table 5).

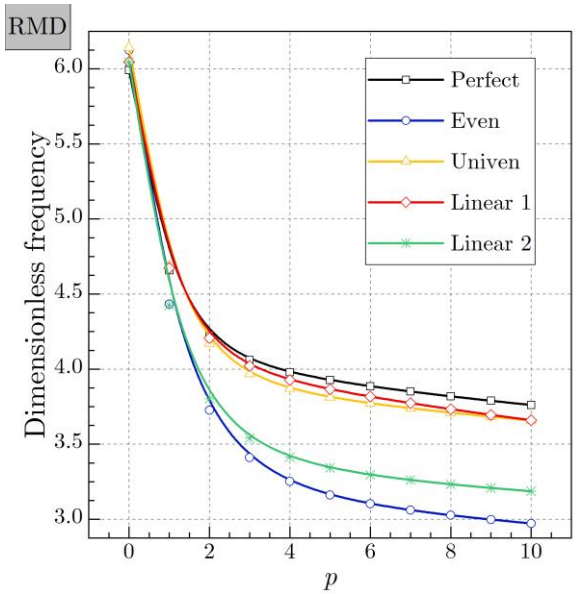

Fig. 5 The effect of the power index "p" and porosity type on the dimensionless frequency (RMD, $a = b = 10h,\ \xi = 0.2, SSSSn = m = 1$)

Table 4 The effect of the geometric parameter "b/a", boundary conditions, and porosity type on the dimensionless frequency ($p = 2, a = b, \xi = 0.1, n = m = 1$)

BCs.	*b*/*a*	Perfect	VFD				RMD			
			Even	Uneven	Nlinear 1	Nlinear 2	Even	Uneven	Nlinear 1	Nlinear 2
SSSS	0,5	9.5811	9.0047	9.4114	9.4466	9.1495	9.0966	9.5228	9.5768	9.1264
	1	4.0090	3.7641	3.9413	3.9544	3.8232	3.8000	3.9901	4.0105	3.8096
	2	2.5365	2.3808	2.4942	2.5022	2.4180	2.4031	2.5255	2.5380	2.4086
	3	2.2598	2.1211	2.2223	2.2293	2.1541	2.1408	2.2502	2.2613	2.1457
	5	2.1177	1.9876	2.0826	2.0892	2.0186	2.0061	2.1088	2.1191	2.0106
CCCC	0,5	17.5733	16.5834	17.2318	17.3073	16.8660	16.7929	17.4222	17.5359	16.8694
	1	7.2633	6.8301	7.1351	7.1610	6.9401	6.9015	7.2207	7.2609	6.9227
	2	5.0176	4.7164	4.9305	4.9477	4.7916	4.7643	4.9907	5.0175	4.7776
	3	4.7236	4.4400	4.6417	4.6578	4.5108	4.4851	4.6984	4.7236	4.4975
	5	4.5984	4.3224	4.5187	4.5344	4.3913	4.3663	4.5740	4.5984	4.3783
CCSS	0,5	10.6913	10.0530	10.4993	10.5397	10.2158	10.1585	10.6224	10.6841	10.1935
	1	5.8497	5.4984	5.7477	5.7681	5.5863	5.5544	5.8174	5.8491	5.5704
	2	4.8277	4.5379	4.7439	4.7604	4.6102	4.5840	4.8018	4.8276	4.5967
	3	4.6620	4.3821	4.5812	4.5971	4.4520	4.4267	4.6372	4.6620	4.4389
	5	4.5809	4.3060	4.5016	4.5172	4.3746	4.3497	4.5567	4.5810	4.3617
CSCS	0,5	16.8210	15.8424	16.5048	16.5741	16.1062	16.0249	16.6905	16.7947	16.0922
	1	7.0556	6.6303	6.9325	6.9573	6.7362	6.6971	7.0162	7.0546	6.7169
	2	4.6707	4.3872	4.5909	4.6065	4.4565	4.4300	4.6474	4.6717	4.4417
	3	4.2808	4.0207	4.2079	4.2220	4.0842	4.0598	4.2598	4.2819	4.0704
	5	4.0935	3.8447	4.0238	4.0373	3.9053	3.8820	4.0736	4.0946	3.8920

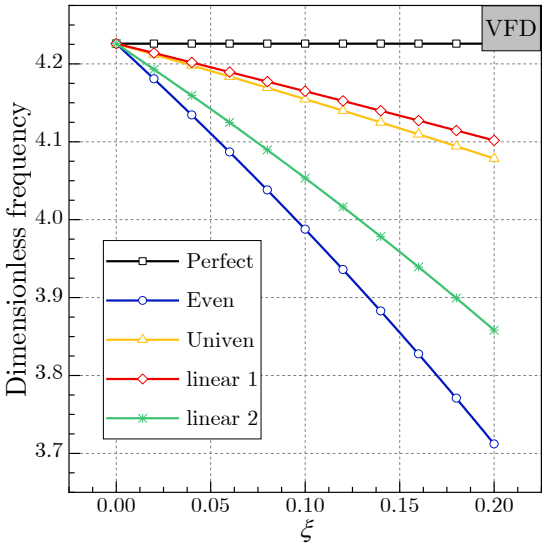

Fig. 6 The effect of the porosity parameter ξ on the dimensionless frequency (VFD) ($p = 2,\ a = b = 10h,$ $SSSS,\ n = m = 1$)

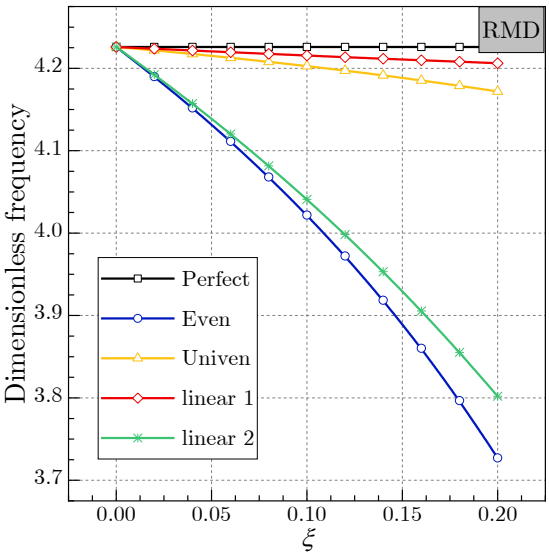

Fig. 7 The effect of the porosity parameter ξ on the dimensionless frequency (RMD) ($p = 2,\ a = b = 10h,$ $SSSS,\ n = m = 1$)

To better observe the influence of these parameters, Figs. 4 to 13 are plotted.

Figs. 4 and 5 represent the effect of the power index "p" and porosity type on the dimensionless frequency of FGM plates, VFD and RMD. For the case of $p = 0$, the plate is entirely ceramic, explaining the highest value of the frequencies due to the high stiffness of the plate in both RMD and VFD cases. As the index p increases, the frequencies decrease critically in the range $0 \leq p \leq 3$, after which the frequencies decrease gradually.

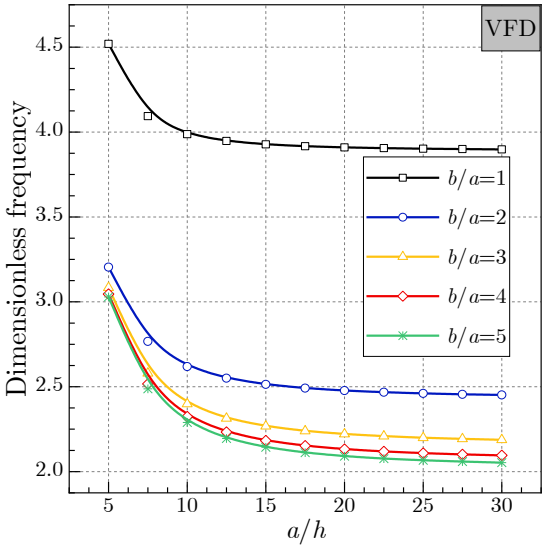

Fig. 8 The effect of the geometric parameters a/h and b/a on the dimensionless frequency (VFD) ($p = 2$, Even, $\xi = 0.1$, $SSSSn = m = 1$)

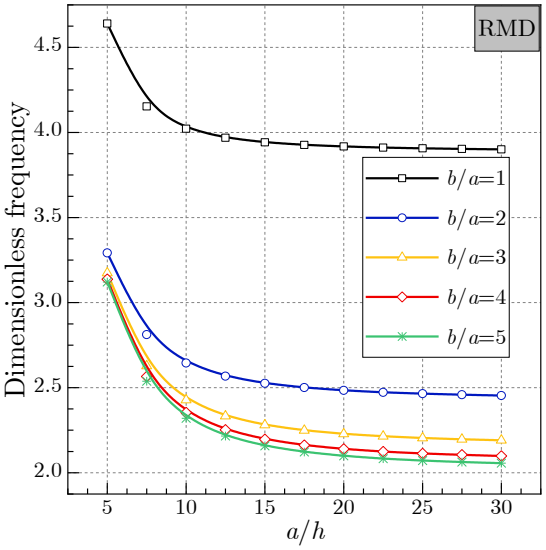

Fig. 9 The effect of the geometric parameters a/h and b/a on the dimensionless frequency (VFD) ($p = 2$, Even, $\xi = 0.1$, $SSSSn = m = 1$)

The maximum values of the frequencies are found in the case of a perfect plate due to the absence of pores. The highest frequencies are found in the case of linear porosity (1), and the lowest values are found in the case of Even porosity.

Based on Figs. 6 and 7, we observe that increasing the porosity coefficient leads to a decrease in the stiffness of the plate and therefore a decrease in the frequencies. This analysis is specific to both RMD and VFD cases. The state of $\xi = 0$ means that the plate does not contain any pores, which

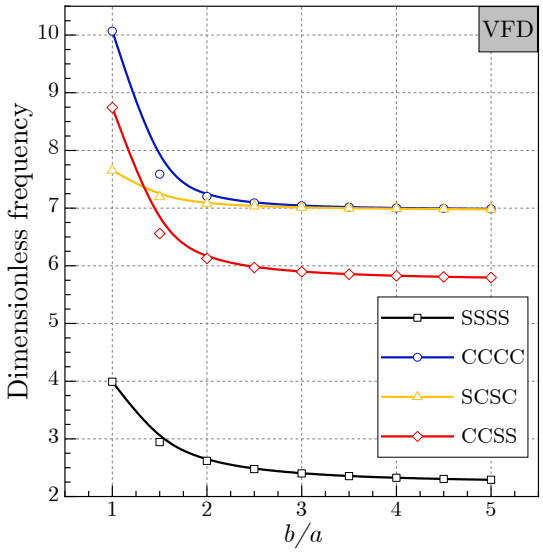

Fig. 10 The effect of boundary conditions and the parameter b/a on the dimensionless frequency (VFD) ($p = 2,\ a = 10h,$ Even, $\xi = 0.1$)

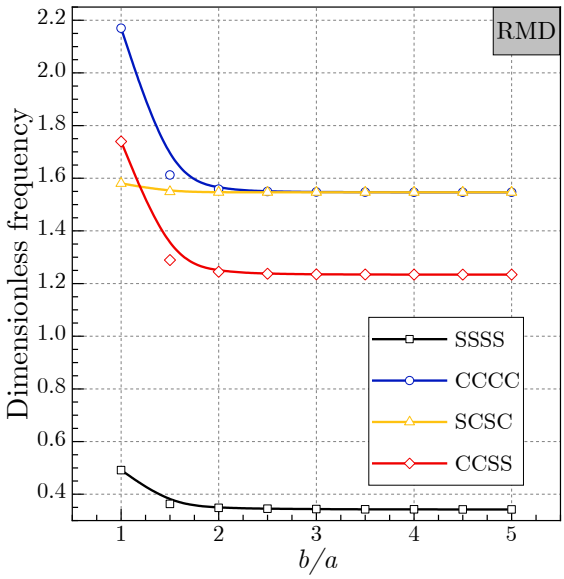

Fig. 11 The effect of boundary conditions and the parameter b/a on the dimensionless frequency (RMD) ($p = 2, a = 10h,$ Even, $\xi = 0.1$)

explains the same frequency for all plates. We can see that the porosity coefficient ξ has a significant effect in the case of linear (2) porosity and the case of Even porosity, compared to the Linear (1) and Uneven cases.

The effect of the geometric parameters a/h and b/a on the dimensionless frequency is presented in Figs. 8 and 9. From these Figs., we can observe that the frequencies increase with the

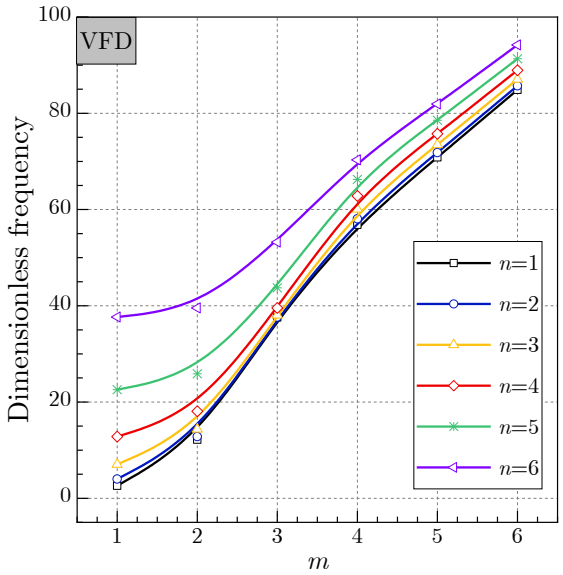

Fig. 12 The effect of the vibration modes m and n on the dimensionless frequency (VFD) ($p = 2, a = b = 10h$, Even, $\xi = 0.1, SSSS$)

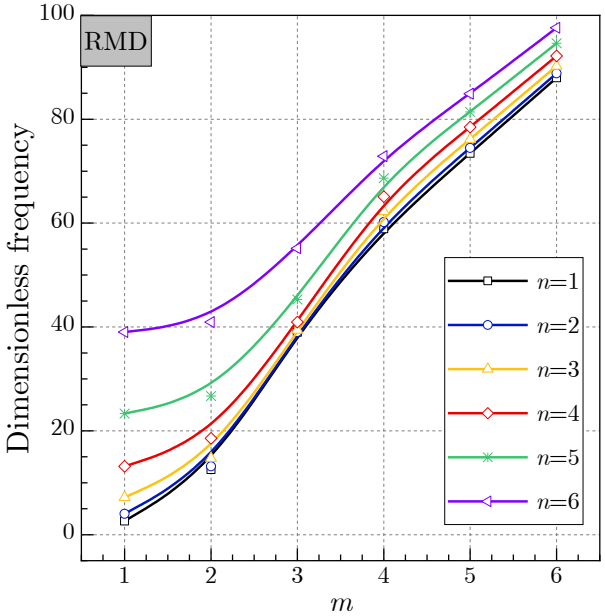

Fig. 13 The effect of the vibration modes m and n on the dimensionless frequency (RMD) ($p = 2, a = b = 10h$, Even, $\xi = 0.1, SSSS$)

increase in both geometric parameters, b/a and a/h. In the case where a/h is greater than 20 ($a/h > 20$), the frequency values become nearly constant.

The effect of the boundary conditions and the parameter b/a on the dimensionless frequency is represented in Figs. 10 and 11. It can be observed that the highest frequency values are seen in

Table 5 The effect of the geometric parameter "a/h" and porosity type on the dimensionless frequency ($p = 2, a = b, \xi = 0.1, SSSS, n = m = 1$)

a/h	Perfect	VFD				RMD			
		Even	Uneven	Nlinear 1	Nlinear 2	Even	Uneven	Nlinear 1	Nlinear 2
5	3.6814	3.4628	3.6138	3.6285	3.5195	3.5001	3.6551	3.6774	3.5136
10	4.0090	3.7641	3.9413	3.9544	3.8232	3.8000	3.9901	4.0105	3.8096
15	4.0829	3.8319	4.0154	4.0279	3.8915	3.8673	4.0661	4.0859	3.8758
20	4.1100	3.8567	4.0426	4.0550	3.9165	3.8920	4.0940	4.1135	3.9001
30	4.1298	3.8749	4.0625	4.0747	3.9347	3.9100	4.1145	4.1337	3.9178

the fixed boundary condition (CCCC), while the lowest values are specific to the simply supported boundary condition (SSSS). As mentioned earlier in Figs. 8 and 9, an increase in the b/a parameter leads to a decrease in frequencies regardless of the boundary conditions. For b/a values greater than 2 ($b/a > 2$), the observation focuses on fixed frequency values.

The effect of the vibration modes *m* and *n* on the dimensionless frequency is examined in Figs. 12 and 13. It can be observed that increasing the vibration modes m and n leads to an increase in the frequencies for both the RMD and VFD cases with different porosity types.

7. Conclusions

In this paper, we have analyzed the vibrational behavior of a functionally graded material (FGM) plate, specifically examining the effects of porosity. We have studied and compared two porosity schemes, VFD and RMD, across four types of porosity distributions for the first time. The primary objective was to explore how these structures respond to vibrations. We used Hamilton's principle to derive the governing equations, which were then solved analytically using the Galerkin method. This research provides a comprehensive analysis of the impacts of material and geometric properties, with the parametric studies demonstrating that:

- Increasing the power index results in a reduction in the stiffness of the FGM plates.
- Incorporating porosities leads to decreased stiffness of the plate, which in turn reduces the dimensionless frequencies.
- Higher porosity coefficients result in lower dimensionless frequencies.
- The dimensionless frequencies of the FGM plate decrease as the geometric parameters b/a and a/h increase.

These findings provide valuable insights into the vibrational behavior of FGM plates with porosities and highlight the importance of considering material properties, geometric parameters, and porosity effects in the design and analysis of such structures.

References

Arshid, E., M. Khorasani, Z. Soleimani-Javid, S. Amir and A. Tounsi (2022), "Porosity-dependent vibration analysis of FG microplates embedded by polymeric nanocomposite patches considering hygrothermal effect via an innovative plate theory", *Eng. Comput.*, **38**(5), 4051-4072. https://doi.org/10.1007/s00366-021-01382-y.

Avcar, M. (2019), "Free vibration of imperfect sigmoid and power law functionally graded beams", *Steel Compos. Struct.*, **30**(6), 603-615. https://doi.org/10.12989/scs.2019.30.6.603

Barati, M.R. (2018), "Porosity-dependent vibration and dynamic stability of compositionally gradient nanofilms using nonlocal strain gradient theory", *Proceedings of the Institution of Mechanical Engineers, Part C: Journal of Mechanical Engineering Science*, **232**(17), 3144-3155. https://doi.org/10.1177/0954406217729421.

Barati, M.R. and H. Shahverdi (2017), "Aero-hygro-thermal stability analysis of higher-order refined supersonic FGM panels with even and uneven porosity distributions", *J. Fl. Struct.*, **73**, 125-136. https://doi.org/10.1016/j.jfluidstructs.2017.06.007.

Bekkaye, T.H.L., B. Fahsi, A.A. Bousahla, F. Bourada, A. Tounsi, K.H. Benrahou, A. Tounsi and M.M. Al-Zahrani (2020), "Porosity-dependent mechanical behaviors of FG plate using refined trigonometric shear deformation theory", *Comput. Concr.*, **26**(5), 439-450.

Belarbi, M.O., A.A. Daikh, A. Garg, H. Hirane, M.S.A. Houari, Ö. Civalek and H.D. Chalak (2022), "Bending and free vibration analysis of porous functionally graded sandwich plate with various porosity distributions using an extended layerwise theory", *Arch. Civil Mech. Eng.*, **23**(1), 15. https://doi.org/10.1007/s43452-022-00551-0.

Belarbi, M.O., Karamanli, A., Benounas, S. and Daikh, A.A. (2024), "Bending, free vibration and buckling finite element analysis of porous functionally graded plates with various porosity distributions using an improved FSDT", *Mech. Based Des. Struct.*, **53**(1), 401-445. https://doi.org/10.1080/15397734.2024.2366530

Belarbi, M.O., S.J. Salami, A. Garg, A.A. Daikh, M.S.A. Houari, R. Dimitri and F. Tornabene (2023), "Mechanical behavior analysis of FG-CNT-reinforced polymer composite beams via a hyperbolic shear deformation theory", *Continuum Mech. Thermodyn.*, **35**(2), 497-520. https://doi.org/10.1007/s00161-023-01191-2.

Daikh, A.A., Houari, M.S.A. and Eltaher, M. (2020), "Nonlocal quasi 3D theory for bending of sigmoid functionally graded sandwich plates under various boundary conditions", *Compos. Struct.*, 113347. https://doi.org/10.1016/j.compstruct.2020.113347.

Daikh, A.A., Houari, M.S.A., Belarbi, M.O., Salwa, M.A., Eltaher, M.A. (2022), "Static and dynamic stability responses of multilayer functionally graded carbon nanotubes reinforced composite nanoplates via quasi 3D nonlocal strain gradient theory", *Defence Technol.*, **18**(10), 1778-1809. https://doi.org/10.1016/j.dt.2021.09.011.

Daikh, A.A. and A.M. Zenkour (2019), "Free vibration and buckling of porous power-law and sigmoid functionally graded sandwich plates using a simple higher-order shear deformation theory", *Mater. Res. Express*, **6**(11), 115707. https://doi.org/10.1088/2053-1591/ab48a9.

Daikh, A.A., M.O. Belarbi, A. Khechai, L. Li, H.M. Ahmed and M.A. Eltaher (2023), "Buckling of bi-coated functionally graded porous nanoplates via a nonlocal strain gradient quasi-3D theory", *Acta Mechanica*, **234**(8), 3397-3420. https://doi.org/10.1007/s00707-023-03548-9.

Daikh, A.A., M.O. Belarbi, A. Khechai, L. Li, S. Khatir, A.A. Abdelrahman and M.A. Eltaher (2023), "Bending of Bi-directional inhomogeneous nanoplates using microstructure-dependent higher-order shear deformation theory", *Eng. Struct.*, **291**, 116230. https://doi.org/10.1016/j.engstruct.2023.116230.

Daikh, A.A., M.O. Belarbi, A. Khechai, L. Li, S. Khatir, A.A. Abdelrahman and M.A. Eltaher (2023), "Bending of Bi-directional inhomogeneous nanoplates using microstructure-dependent higher-order shear deformation theory", *Eng. Struct.*, **291**, 116230. https://doi.org/10.1016/j.engstruct.2023.116230.

Daikh, A.A., M.O. Belarbi, D. Ahmed, M.S.A. Houari, M. Avcar, A. Tounsi and M.A. Eltaher (2023), "Static analysis of functionally graded plate structures resting on variable elastic foundation under various boundary conditions", *Acta Mechanica*, **234**(2), 775-806. https://doi.org/10.1007/s00707-022-03405-1.

Demirhan, P.A. and V. Taskin. (2019), "Bending and free vibration analysis of levy-type porous functionally graded plate using state space approach", *Compos. Part B Eng.*, **160**, 661-676. https://doi.org/10.1016/j.compositesb.2018.12.020

Demirhan, P.A. and V. Taskin (2019), "Bending and free vibration analysis of Levy-type porous functionally graded plate using state space approach", *Compos. Part B Eng.*, **160**, 661-676.

https://doi.org/10.1016/j.compositesb.2018.12.020.
Gafour, Y., A. Hamidi, A. Benahmed, M. Zidour and T. Bensattalah (2020), "Porosity-dependent free vibration analysis of FG nanobeam using non-local shear deformation and energy principle", *Adv. Nano Res.*, **8**(1), 49. https://doi.org/10.12989/anr.2020.8.1.037
Garg, A., M.O. Belarbi, H.D. Chalak and A. Chakrabarti (2021), "A review of the analysis of sandwich FGM structures", *Compos. Struct.*, **258**, 113427. https://doi.org/10.1016/j.compstruct.2020.113427.
Ghandourah, E.E., Daikh, A.A., Khatir, S., Alhawsawi, A.M., Banoqitah, E.M., Eltaher, M.A. (2023), "A dynamic analysis of porous coated functionally graded nanoshells rested on viscoelastic medium", *Mathematics*, **11**(10), 2407. https://doi.org/10.3390/math11102407.
Hai Van, N.T. and N.T. Hong (2023), "Novel finite element modeling for free vibration and buckling analysis of non-uniform thickness 2D-FG sandwich porous plates using refined Quasi 3D theory", *Mech. Based Des. Struct.*, **52**(6), 3052-3078. https://doi.org/10.1080/15397734.2023.2197035.
Hirane, H., M.O. Belarbi, M.S.A. Houari and A. Tounsi (2021), "On the layerwise finite element formulation for static and free vibration analysis of functionally graded sandwich plates", *Eng. Comput.*, 1-29. https://doi.org/10.1007/s00366-020-01250-1.
Hu, Z., Shi, Y., Xiong, S., Zheng, X. and Li, R. (2023), "New analytic free vibration solutions of non-Lévy-type porous FGM rectangular plates within the symplectic framework", *Thin Wall. Struct.*, **185**, 110609. https://doi.org/10.1016/j.tws.2023.110609
Khechai, A., A. Tati, M.O. Belarbi and A. Guettala (2015), *Finite Element Analysis of Stress Concentrations in Isotropic and Composite Plates with Elliptical Holes*, In *Design and Modeling of Mechanical Systems – II*, Cham: Springer International Publishing.
Kumar, P. and S.P. Harsha (2022), "Dynamic analysis of porosity dependent functionally graded sigmoid piezoelectric (FGSP) plate", *Structures*, **46**, 1737-1752. https://doi.org/10.1016/j.istruc.2022.11.021.
Li, H., F. Pang, H. Chen and Y. Du (2019), "Vibration analysis of functionally graded porous cylindrical shell with arbitrary boundary restraints by using a semi analytical method", *Compos. Part B Eng.*, **164**, 249-264. https://doi.org/10.1016/j.compositesb.2018.11.046.
Li, S., S. Zheng and D. Chen (2020), "Porosity-dependent isogeometric analysis of bi-directional functionally graded plates", *Thin Wall. Struct.*, **156**, 106999. https://doi.org/10.1016/j.tws.2020.106999.
Merdaci, S. and H. Belghoul (2019), "High-order shear theory for static analysis of functionally graded plates with porosities", *Comptes Rendus Mécanique*, **347**(3), 207-217. https://doi.org/10.1016/j.crme.2019.01.001.
Mohamed, S.A., A.E. Assie and M.A. Eltaher (2023), "Novel incremental procedure in solving nonlinear static response of 2D-FG porous plates", *Thin Wall. Struct.*, **189**, 110779. https://doi.org/10.1016/j.tws.2023.110779.
Rezaei, A.S., A.R. Saidi, M. Abrishamdari and M.H.P. Mohammadi (2017), "Natural frequencies of functionally graded plates with porosities via a simple four variable plate theory: An analytical approach", *Thin Wall. Struct.*, **120**, 366-377. https://doi.org/10.1016/j.tws.2017.08.003.
Saffari, P.R., C. Thongchom, T. Jearsiripongkul, P.R. Saffari, S. Keawsawasvong and S. Kongwat (2023), "Porosity-dependent wave propagation in multi-directional functionally graded nanoplate with nonlinear temperature-dependent characteristics on Kerr-type substrate", *Int. J. Thermofl.*, **20**, 100408. https://doi.org/10.1016/j.ijft.2023.100408.
Saleh, B., J. Jiang, R. Fathi, T. Al-hababi, Q. Xu, L. Wang, D. Song and A. Ma (2020), "30 Years of functionally graded materials: An overview of manufacturing methods, Applications and Future Challenges", *Compos. Part B Eng.*, **201**, 108376. https://doi.org/10.1016/j.compositesb.2020.108376.
Shahsavari, D., M. Shahsavari, L. Li and B. Karami (2018), "A novel quasi-3D hyperbolic theory for free vibration of FG plates with porosities resting on Winkler/Pasternak/Kerr foundation", *Aerosp. Sci. Technol.*, **72**, 134-149. https://doi.org/10.1016/j.ast.2017.11.004.
Shahverdi, H. and M.R. Barati (2017), "Vibration analysis of porous functionally graded nanoplates", *Int. J. Eng. Sci.*, **120**, 82-99. https://doi.org/10.1016/j.ijengsci.2017.06.008.
Thanh, C.L., Nguyen, K.D., Le-Minh, H., Phan-Vu, P., Nguyen-Trong, P. and Tounsi, A. (2022), "Nonlinear bending analysis of porous sigmoid FGM nanoplate via IGA and nonlocal strain gradient theory", *Adv.*

Nano Res., **12**(5), 441-455. https://doi.org/10.12989/anr.2022.12.5.441

Thanh, C.L., Nguyen, K.D., Nguyen-Trong, N., Khatir, S., Nguyen-Xuan, H. and Abdel-Wahab, M. (2021), "A three-dimensional solution for free vibration and buckling of annular plate, conical, cylinder and cylindrical shell of FG porous-cellular materials using IGA", *Compos. Struct*., **259**, 113216. https://doi.org/10.1016/j.compstruct.2020.113216

Thanh, C.L., Nguyen, T.N., Vu, T.H., Khatir, S. and Abdel-Wahab, M. (2022), "A geometrically nonlinear size-dependent hypothesis for porous functionally graded micro-plate", *Eng. Comput*., **38**(Suppl 1), 449-460. https://doi.org/10.1007/s00366-020-01154-0

Thanh, C.L., Tran, L.V., Bui, T.Q., Nguyen, H.X. and Abdel-Wahab, M. (2019), "Isogeometric analysis for size-dependent nonlinear thermal stability of porous FG microplates", *Compos. Struct*., **221**, 110838. https://doi.org/10.1016/j.compstruct.2019.04.010

Tran, T.T., Q.H. Pham and T. Nguyen-Thoi (2021), "Static and free vibration analyses of functionally graded porous variable-thickness plates using an edge-based smoothed finite element method", *Defence Technol*., **17**(3), 971-986. https://doi.org/10.1016/j.dt.2020.06.001.

Van Do, V.N. and C.H. Lee (2023), "Bending and instability behaviour of functionally graded cylindrical shells with porosities", *Acta Mechanica*, **234**(5), 1811-1842. https://doi.org/10.1007/s00707-023-03475-9.

Van Vinh, P., A. Tounsi and M.O. Belarbi (2023), "On the nonlocal free vibration analysis of functionally graded porous doubly curved shallow nanoshells with variable nonlocal parameters", *Eng. Comput*., **39**(1), 835-855. https://doi.org/10.1007/s00366-022-01687-6.

Van Vinh, P., M.O. Belarbi, M. Avcar and Ö. Civalek (2023), "An improved first-order mixed plate element for static bending and free vibration analysis of functionally graded sandwich plates", *Arch. Appl. Mech*., **93**(5), 1841-1862. https://doi.org/10.1007/s00419-022-02359-z.

Van Vinh, P., N. Van Chinh and A. Tounsi (2022), "Static bending and buckling analysis of bi-directional functionally graded porous plates using an improved first-order shear deformation theory and FEM", *Eur. J. Mech. A Solids*, **96**, 104743. https://doi.org/10.1016/j.euromechsol.2022.104743.

Wang, Y.Q. and J.W. Zu (2017), "Porosity-dependent nonlinear forced vibration analysis of functionally graded piezoelectric smart material plates", *Smart Mater. Struct*., **26**(10), 105014. https://doi.org/10.1088/1361-665X/aa8429.

Woo, J., Meguid, S., Liew, K. (2003), "Thermomechanical postbuckling analysis of functionally graded plates and shallow cylindrical shells", *Acta Mechanica*, **165**, 99-115. https://doi.org/10.1007/s00707-003-0035-4.

Xia, Q., Xiang, P., Jiang, L., Yan, J. and Peng, L. (2022), "Bending and free vibration analysis of laminated plates on Winkler foundations based on meshless layerwise theory", *Mech. Adv. Mater. Struct*., **29**(27), 6168-6187. https://doi.org/10.1080/15376494.2021.1972497

Xia, Q., Xiang, P., Peng, L., Wang, H. and Jiang, L. (2024), "Interlayer shearing and bending performances of ballastless track plates based on high-order shear deformation theory (HSDT) for laminated structures", *Mech. Adv. Mater. Struct*., **31**(7), 1563-1587. https://doi.org/10.1080/15376494.2022.2139441

Xiang, P., Xia, Q., Jiang, L.Z., Peng, L., Yan, J.W. and Liu, X. (2021), "Free vibration analysis of FG-CNTRC conical shell panels using the kernel particle Ritz element-free method", *Compos. Struct*., **255**, 112987. https://doi.org/10.1016/j.compstruct.2020.112987

Xiang, P., Zhang, L.W. and Liew, K.M. (2016), "Meshfree simulation of temperature effects on the mechanical behaviors of microtubules", *Eng. Anal. Bound. Elem*., **69**, 104-118. https://doi.org/10.1016/j.enganabound.2016.05.006

Xue, Y., G. Jin, X. Ma, H. Chen, T. Ye, M. Chen and Y. Zhang (2019), "Free vibration analysis of porous plates with porosity distributions in the thickness and in-plane directions using isogeometric approach", *Int. J. Mech. Sci*., **152**, 346-362. https://doi.org/10.1016/j.ijmecsci.2019.01.004.

Yahia, S.A., H.A. Atmane, M.S.A. Houari, A.J.S.E. Tounsi (2015), "Wave propagation in functionally graded plates with porosities using various higher-order shear deformation plate theories", *Struct. Eng. Mech*., **53**(6), 1143-1165. https://doi.org/10.12989/sem.2015.53.6.1143.

Zenkour, A.M. and M.H. Aljadani (2019), "Porosity effect on thermal buckling behavior of actuated functionally graded piezoelectric nanoplates", *Eur. J. Mech. A Solids*, **78**, 103835. https://doi.org/10.1016/j.euromechsol.2019.103835.

Zhang, Y., G. Jin, M. Chen, T. Ye, C. Yang and Y. Yin (2020), "Free vibration and damping analysis of porous functionally graded sandwich plates with a viscoelastic core", *Compos. Struct.*, **244**, 112298. https://doi.org/10.1016/j.compstruct.2020.112298.

Zhou, K., X. Huang, J. Tian and H. Hua (2018), "Vibration and flutter analysis of supersonic porous functionally graded material plates with temperature gradient and resting on elastic foundation", *Compos. Struct.*, **204**, 63-79. https://doi.org/10.1016/j.compstruct.2018.07.057.

Zhu, J., Z. Lai, Z. Yin, J. Jeon and S. Lee (2001), "Fabrication of ZrO2–NiCr functionally graded material by powder metallurgy", *Mater. Chem. Phys.*, **68**(1), 130-135. https://doi.org/10.1016/S0254-0584(00)00355-2.

CC

Appendix

Stiffness matrix [K] elements:

$$K_{11} = A_{11}\int_0^a\int_0^b \frac{\partial^3 X_m}{\partial x^3} Y_n \frac{\partial X_m}{\partial x} Y_n \,\mathrm{d}x\mathrm{d}y + A_{66}\int_0^a\int_0^b \frac{\partial X_m}{\partial x}\frac{\partial^2 Y_n}{\partial y^2}\frac{\partial X_m}{\partial x} Y_n \,\mathrm{d}x\mathrm{d}y$$

$$K_{12} = (A_{12} + A_{66})\int_0^a\int_0^b \frac{\partial X_m}{\partial x}\frac{\partial^2 Y_n}{\partial y^2}\frac{\partial X_m}{\partial x} Y_n \,\mathrm{d}x\mathrm{d}y$$

$$K_{13} = B_{11}\int_0^a\int_0^b \frac{\partial^3 X_m}{\partial x^3} Y_n \frac{\partial X_m}{\partial x} Y_n \,\mathrm{d}x\mathrm{d}y - (B_{12} + 2B_{66})\int_0^a\int_0^b \frac{\partial X_m}{\partial x}\frac{\partial^2 Y_n}{\partial y^2}\frac{\partial X_m}{\partial x} Y_n \,\mathrm{d}x\mathrm{d}y$$

$$K_{14} = B_{11}^s\int_0^a\int_0^b \frac{\partial^3 X_m}{\partial x^3} Y_n \frac{\partial X_m}{\partial x} Y_n \,\mathrm{d}x\mathrm{d}y + B_{66}^s\int_0^a\int_0^b \frac{\partial X_m}{\partial x}\frac{\partial^2 Y_n}{\partial y^2}\frac{\partial X_m}{\partial x} Y_n \,\mathrm{d}x\mathrm{d}y$$

$$K_{15} = (B_{12}^s + B_{66}^s)\int_0^a\int_0^b \frac{\partial X_m}{\partial x}\frac{\partial^2 Y_n}{\partial y^2}\frac{\partial X_m}{\partial x} Y_n \,\mathrm{d}x\mathrm{d}y$$

$$K_{21} = (A_{12} + A_{66})\int_0^a\int_0^b \frac{\partial^2 X_m}{\partial x^1}\frac{\partial Y_n}{\partial y} X_m \frac{\partial Y_n}{\partial y} \mathrm{d}x\mathrm{d}y$$

$$K_{22} = A_{22}\int_0^a\int_0^b X_m \frac{\partial^3 Y_n}{\partial y^3} X_m \frac{\partial Y_n}{\partial y} \mathrm{d}x\mathrm{d}y + A_{66}\int_0^a\int_0^b\int_0^b \frac{\partial^2 X_m}{\partial x^2}\frac{\partial Y_n}{\partial y} X_m \frac{\partial Y_n}{\partial y} \mathrm{d}x\mathrm{d}y$$

$$K_{23} = B_{22}\int_0^a\int_0^b X_m \frac{\partial^3 Y_n}{\partial y^3} X_m \frac{\partial Y_n}{\partial y} \mathrm{d}x\mathrm{d}y - (B_{12} + 2B_{66})\int_0^a\int_0^b \frac{\partial^2 X_m}{\partial x^2}\frac{\partial Y_n}{\partial y} X_m \frac{\partial Y_n}{\partial y} \mathrm{d}x\mathrm{d}y$$

$$K_{24} = (B_{12}^s + B_{66}^s)\int_0^a\int_0^b \frac{\partial^2 X_m}{\partial x^2}\frac{\partial Y_n}{\partial y} X_m \frac{\partial Y_n}{\partial y} \mathrm{d}x\mathrm{d}y$$

$$K_{25} = B_{22}^{s}\int_0^a\int_0^b X_m\frac{\partial^3 Y_n}{\partial y^3}X_m\frac{\partial Y_n}{\partial y}\mathrm{d}x\mathrm{d}y + B_{66}^{s}\int_0^a\int_0^b \frac{\partial^2 X_m}{\partial x^2}\frac{\partial Y_n}{\partial y}X_m\frac{\partial Y_n}{\partial y}\mathrm{d}x\mathrm{d}y$$

$$K_{31} = B_{11}\int_0^a\int_0^b \frac{\partial^4 X_n}{\partial x^4}Y_nX_mY_n\,\mathrm{d}x\mathrm{d}y + (B_{12}+2B_{66})\int_0^a\int_0^b \frac{\partial^2 X_m}{\partial x^2}\frac{\partial^2 Y_n}{\partial y^2}X_mY_n\,\mathrm{d}x\mathrm{d}y$$

$$K_{32} = B_{22}\int_0^a\int_0^b X_m\frac{\partial^4 Y_n}{\partial y^4}X_mY_n\,\mathrm{d}x\mathrm{d}y + (B_{12}+2B_{66})\int_0^a\int_0^b \frac{\partial^2 X_m}{\partial x^2}\frac{\partial^2 Y_n}{\partial y^2}X_mY_n\,\mathrm{d}x\mathrm{d}y$$

$$K_{33} = -D_{11}\int_0^a\int_0^b \frac{\partial^4 X_m}{\partial x^4}Y_nX_mY_n\,\mathrm{d}x\mathrm{d}y - D_{22}\int_0^a\int_0^b X_m\frac{\partial^4 Y_n}{\partial y^4}X_mY_n\,\mathrm{d}x\mathrm{d}y - 2(D_{12}+2D_{66})\int_0^a\int_0^b \frac{\partial^2 X_m}{\partial x^2}\frac{\partial^2 Y_n}{\partial y^2}X_mY_n\,\mathrm{d}x\mathrm{d}y$$

$$K_{34} = D_{11}^{s}\int_0^a\int_0^b \frac{\partial^4 X_m}{\partial x^4}Y_nX_mY_n\,\mathrm{d}x\mathrm{d}y + (D_{12}^{s}+2D_{66}^{s})\int_0^a\int_0^b \frac{\partial^2 X_m}{\partial x^2}\frac{\partial^2 Y_n}{\partial y^2}X_mY_n\,\mathrm{d}x\mathrm{d}y$$

$$K_{35} = D_{22}^{s}\int_0^a\int_0^b X_m\frac{\partial^4 Y_n}{\partial y^4}X_mY_n\,\mathrm{d}x\mathrm{d}y + (D_{12}^{s}+2D_{66}^{s})\int_0^a\int_0^b \frac{\partial^2 X_m}{\partial x^2}\frac{\partial^2 Y_n}{\partial y^2}X_mY_n\,\mathrm{d}x\mathrm{d}y$$

$$K_{41} = B_{11}^{s}\int_0^a\int_0^b \frac{\partial^3 X_m}{\partial x^3}Y_n\frac{\partial X_m}{\partial x}Y_n\,\mathrm{d}x\mathrm{d}y + B_{66}^{s}\int_0^a\int_0^b \frac{\partial X_m}{\partial x}\frac{\partial^2 Y_n}{\partial y^2}\frac{\partial X_m}{\partial x}Y_n\,\mathrm{d}x\mathrm{d}y$$

$$K_{42} = (B_{12}^{s}+B_{66}^{s})\int_0^a\int_0^b \frac{\partial X_m}{\partial x}\frac{\partial^2 Y_n}{\partial y^2}\frac{\partial X_m}{\partial x}Y_n\,\mathrm{d}x\mathrm{d}y$$

$$K_{43} = -D_{11}^{s}\int_0^a\int_0^b \frac{\partial^3 X_m}{\partial x^3}Y_n\frac{\partial X_m}{\partial x}Y_n\,\mathrm{d}x\mathrm{d}y - (D_{12}^{s}+2D_{66}^{s})\int_0^a\int_0^b \frac{\partial X_m}{\partial x}\frac{\partial^2 Y_n}{\partial y^2}\frac{\partial X_m}{\partial x}Y_n\,\mathrm{d}x\mathrm{d}y$$

$$K_{44} = F_{11}^{s}\int_0^a\int_0^b \frac{\partial^3 X_m}{\partial x^3}Y_n\frac{\partial X_m}{\partial x}Y_n\,\mathrm{d}x\mathrm{d}y + F_{66}^{s}\int_0^a\int_0^b \frac{\partial X_m}{\partial x}\frac{\partial^2 Y_n}{\partial y^2}\frac{\partial X_m}{\partial x}Y_n\,\mathrm{d}x\mathrm{d}y - A_{44}^{s}\int_0^a\int_0^b \frac{\partial X_m}{\partial x}Y_n\frac{\partial X_m}{\partial x}Y_n\,\mathrm{d}x\mathrm{d}y$$

$$K_{45} = (F_{12}^{s}+F_{66}^{s})\int_0^a\int_0^b \frac{\partial X_m}{\partial x}\frac{\partial^2 Y_n}{\partial y^2}\frac{\partial X_m}{\partial x}Y_n\,\mathrm{d}x\mathrm{d}y$$

$$K_{51} = (B_{12}^{s}+B_{66}^{s})\int_0^a\int_0^b \frac{\partial^2 X_m}{\partial x^2}\frac{\partial Y_n}{\partial y}X_m\frac{\partial Y_n}{\partial y}\mathrm{d}x\mathrm{d}y$$

$$K_{52} = B_{22}^{s}\int_0^a\int_0^b X_m\frac{\partial^3 Y_n}{\partial y^3}X_m\frac{\partial Y_n}{\partial y}\mathrm{d}x\mathrm{d}y + B_{66}^{s}\int_0^a\int_0^b \frac{\partial^2 X_m}{\partial x^2}\frac{\partial Y_n}{\partial y}X_m\frac{\partial Y_n}{\partial y}\mathrm{d}x\mathrm{d}y$$

$$K_{53} = -D_{22}^{s}\int_0^a\int_0^b X_m\frac{\partial^3 Y_n}{\partial y^3}X_m\frac{\partial Y_n}{\partial y}\mathrm{d}x\mathrm{d}y - (D_{12}^{s}+2D_{66}^{s})\int_0^a\int_0^b \frac{\partial^2 X_m}{\partial x^2}\frac{\partial Y_n}{\partial y}X_m\frac{\partial Y_n}{\partial y}\mathrm{d}x\mathrm{d}y$$

$$K_{54} = (F_{12}^{s}+F_{66}^{s})\int_0^a\int_0^b \frac{\partial^2 X_m}{\partial x^2}\frac{\partial Y_n}{\partial y}X_m\frac{\partial Y_n}{\partial y}\mathrm{d}x\mathrm{d}y$$

$$K_{55} = F_{22}^{s}\int_0^a\int_0^b X_m\frac{\partial^3 Y_n}{\partial y^3}X_m\frac{\partial Y_n}{\partial y}\mathrm{d}x\mathrm{d}y + F_{66}^{s}\int_0^a\int_0^b \frac{\partial^2 X_m}{\partial x^2}\frac{\partial Y_n}{\partial y}X_m\frac{\partial Y_n}{\partial y}\mathrm{d}x\mathrm{d}y - A_{55}^{s}\int_0^a\int_0^b X_m\frac{\partial Y_n}{\partial y}X_m\frac{\partial Y_n}{\partial y}\mathrm{d}x\mathrm{d}y$$

Mass matrix [M] elements;

$$M_{11} = I_0\int_0^a\int_0^b \frac{\partial X_m}{\partial x}Y_n\frac{\partial X_m}{\partial x}Y_n\,\mathrm{d}x\mathrm{d}y$$

$$M_{13} = -I_1 - \int_0^a\int_0^b \frac{\partial X_m}{\partial x}Y_n\frac{\partial X_m}{\partial x}Y_n\,\mathrm{d}x\mathrm{d}y$$

$$M_{14} = I_3\int_0^a\int_0^b \frac{\partial X_m}{\partial x}Y_n\frac{\partial X_m}{\partial x}Y_n\,\mathrm{d}x\mathrm{d}y$$

$$M_{22} = I_0\int_0^a\int_0^b X_m\frac{\partial Y_n}{\partial y}X_m\frac{\partial Y_n}{\partial y}\mathrm{d}x\mathrm{d}y$$

$$M_{23} = -I_1\int_0^a\int_0^b X_m\frac{\partial Y_n}{\partial y}X_m\frac{\partial Y_n}{\partial y}\mathrm{d}x\mathrm{d}y$$

$$M_{25} = -I_3\int_0^a\int_0^b X_m\frac{\partial Y_n}{\partial y}X_m\frac{\partial Y_n}{\partial y}\mathrm{d}x\mathrm{d}y$$

$$M_{31} = I_1\int_0^a\int_0^b \frac{\partial^2 X_m}{\partial x^2}Y_nX_mY_n\,\mathrm{d}x\mathrm{d}y$$

$$M_{32} = I_1I_1\int_0^a\int_0^b X_m\frac{\partial^2 Y_n}{\partial y^2}X_mY_n\,\mathrm{d}x\mathrm{d}y$$

$$M_{33} = I_0\int_0^a\int_0^b X_mY_nX_mY_n\,\mathrm{d}x\mathrm{d}y - I_2\left(\int_0^a\int_0^b \frac{\partial^2 X_m}{\partial x^2}Y_nX_mY_n\,\mathrm{d}x\mathrm{d}y + \int_0^a\int_0^b X_m\frac{\partial^2 Y_n}{\partial y^2}X_mY_n\,\mathrm{d}x\mathrm{d}y\right)$$

$$M_{34} = -I_4 \int_0^a \int_0^b \frac{\partial^2 X_m}{\partial x^2} Y_n X_m Y_n \, \mathrm{d}x\mathrm{d}y$$

$$M_{34} = -I_4 \int_0^a \int_0^b X_m \frac{\partial^2 Y_n}{\partial y^2} X_m Y_n \, \mathrm{d}x\mathrm{d}y$$

$$M_{41} = I_3 \int_0^a \int_0^b \frac{\partial X_m}{\partial x} Y_n \frac{\partial X_m}{\partial x} Y_n \, \mathrm{d}x\mathrm{d}y$$

$$M_{43} = -I_4 \int_0^a \int_0^b \frac{\partial X_m}{\partial x} Y_n \frac{\partial X_m}{\partial x} Y_n \, \mathrm{d}x\mathrm{d}y$$

$$M_{44} = I_5 \int_0^a \int_0^b \frac{\partial X_m}{\partial x} Y_n \frac{\partial X_m}{\partial x} Y_n \, \mathrm{d}x\mathrm{d}y$$

$$M_{52} = I_3 \int_0^a \int_0^b X_m \frac{\partial Y_n}{\partial y} X_m \frac{\partial Y_n}{\partial y} \mathrm{d}x\mathrm{d}y$$

$$M_{53} = -I_4 \int_0^a \int_0^b X_m \frac{\partial Y_n}{\partial y} X_m \frac{\partial Y_n}{\partial y} \mathrm{d}x\mathrm{d}y$$

$$M_{55} = -I_5 \int_0^a \int_0^b X_m \frac{\partial Y_n}{\partial y} X_m \frac{\partial Y_n}{\partial y} \mathrm{d}x\mathrm{d}y$$

$$M_{12} = M_{15} = M_{21} = M_{24} = M_{42} = M_{45} = M_{51} = M_{54} = 0$$